Biomed Tech 2009; 54:48–54 © 2009 by Walter de Gruyter • Berlin • New York. DOI 10.1515/BMT.2009.007

Short communication

Post-processing technique for improved assessment of hard tissues in the submicrometer domain using local synchrotron radiation-based computed tomography

Nachbearbeitungstechnik für eine verbesserte Erfassung harten Gewebes im Submikrometerbereich mittels lokaler synchrotronstrahlungsbasierter Computertomographie

Philipp Schneider[1], Romain Voide[1], Marco Stampanoni[2] and Ralph Müller[1,*]

[1] Institute for Biomedical Engineering, University and ETH Zurich, Zurich, Switzerland

[2] Swiss Light Source (SLS), Paul Scherrer Institut (PSI), Villigen, Switzerland

Abstract

During the last two decades micro-computed tomography has become the method of choice for the non-destructive assessment and quantitative morphometry of hard tissues in three dimensions. With the advent of third-generation synchrotron radiation sources, micro-computed tomography in the micrometer range has become feasible and has been employed to analyze local bone tissue properties. However, owing to limitations regarding the tradeoff between object size and spatial resolution, non-destructive conventional global computed tomography of hard tissues, such as bone, remains unachievable in the submicrometer domain so far. Here, we report on a post-processing technique for the assessment of hard tissues using local synchrotron radiation-based computed tomography, which overcomes this experimental limitation.

Keywords: bone ultrastructure; canal network; cortical bone; cupping; morphometry; mouse; osteocyte lacunae.

Zusammenfassung

Hinsichtlich einer zerstörungsfreien Erfassung und quantitativen Morphometrie harten Gewebes in drei Dimensionen hat sich die Mikro-Computertomographie im Verlaufe der letzten zwei Jahrzehnte zur Methode der Wahl entwickelt. Mit dem Aufkommen von Synchrotronstrahlungsquellen der dritten Generation wurde Mikro-Computertomographie im Mikrometerbereich möglich und angewandt, um lokale Knocheneigenschaften zu untersuchen. Jedoch bleibt – infolge von Beschränkungen hinsichtlich des Kompromisses zwischen Objektgröße und Ortsauflösung – zerstörungsfreie herkömmliche globale Computertomographie für hartes Gewebe wie Knochen im Submikrometerbereich bis heute unerreichbar. An dieser Stelle berichten wir über eine Nachbearbeitungstechnik für die Erfassung harten Gewebes im Submikrometerbereich mittels synchrotronstrahlungsbasierter lokaler Computertomographie, die diese experimentelle Beschränkung überwindet.

Schlüsselwörter: Cupping; kannuläres Netzwerk; Knochen-Ultrastruktur; kortikaler Knochen; Maus; Morphometrie; Osteozyt-Lakunen.

Bone architecture has traditionally been studied by optical microscopy, based on two-dimensional (2D) histomorphometry. Classical bone histomorphometry involves embedding and serial sectioning of the sample, which is laborious as well as destructive, and additionally, implies model assumptions for the computation of three-dimensional (3D) morphometric indices, as it is inherently a 2D technique. In comparison [21], micro-computed tomography (μCT) overcomes these limitations, because it is a non-destructive and truly 3D technique. Moreover, the continuously increasing spatial resolution capabilities of CT systems provide a more detailed insight into bone tissue. For instance, several authors have recently assessed and partly quantified the canal network within human cortical bone [4, 6, 12].

Currently, synchrotron radiation (SR) facilities offer CT systems running at spatial resolutions down to around 1 μm [20] and novel techniques are under development [26] for CT even below 100 nm. A typical experimental station dedicated to SR μCT [29] operates at present in its standard mode as a transmission microscope for a low-divergence X-ray beam, where the magnified microradiographic projections of the specimen are captured by a charge coupled device (CCD), after being converted by a transparent luminescent screen (scintillator) into visible light. According to this experimental setup, the spatial resolution of such a system is consequently limited by wave-front aberrations arising from the depth of focus (or defect of focus) as well as by diffraction and spherical aberrations owing to the thickness of the scintillator and its substrate [15]. As a result, the combination of scintil-

*Corresponding author: Prof. Dr. Ralph Müller, Institute for Biomechanics, ETH Zurich, Wolfgang-Pauli-Strasse 10, 8093 Zürich, Switzerland
Phone: +41-44-632-4592
Fax: +41-44-632-1214
E-mail: ram@ethz.ch

lators with optical magnification allows SR CT down to resolutions of a few hundred nanometers.

However, SR CT systems are only rarely used close to their full resolution capacity for the examination of biological specimens [7, 23, 31]. This is primarily due to the fact that for a given CCD with a fixed pixel array, every increase in magnification of the optical system is accompanied by an equal reduction in the fraction of the recorded sample projection, i.e., by a decrease in the field of view (FOV). In other words, the maximal sample size that can be assessed by current SR CT setups in their standard mode is limited by the magnification of the optical system. Namely, the most popular category of CCD cameras presently in use for SR CT applications [20] are equipped with an image area of up to 2048×2048 pixels and thus restrict the sample diameter to less than 1 mm in cross-section for observations at a theoretical pixel size below 0.5 μm or for a corresponding spatial resolution on the order of 1 μm, respectively. Since intact (biological) specimens are typically larger than 1 mm, this constraint prevents non-destructive investigations in the micrometer and submicrometer regime.

A straightforward approach to tackle this limitation is to focus exclusively on a fraction of the specimen by cutting it physically to a size smaller than the maximal FOV. To evaluate this first approach for bone tissue, we excised a cortical sector from the femoral mid-diaphysis of a mouse using a scalpel. The bone section was then measured at the X-ray Tomographic Microscopy (XTM) station [29] of the Materials Science (MS) beamline at the Swiss Light Source (SLS) at a theoretical pixel size of 350 nm. A reconstructed slice of the cortical bone is shown in Figure 1A and B, where the canal network and the osteocyte lacunar system are clearly visible. At the same time, Figure 1A illustrates that cutting the bone tissue causes initiation and progression of fractures, which eventually lead to the separation of bone fragments and which are in diametrical opposition to the advantage of CT as a non-destructive imaging technique. Moreover, the selection and mechanical dissection of a predefined bone site becomes a challenging task for sample dimensions of a few hundred micrometers only. Finally, the integrity of bone specimens cut for CT measurement is destroyed and any subsequent histomorphometric examination is precluded at the outset. For all these reasons, mechanical reduction of the sample size as presented beforehand is undesirable for submicrometer SR CT.

Here, we present an alternative strategy, where we developed a post-processing technique for non-destructive local SR CT operating at a theoretical pixel size in the submicrometer regime, which can be implemented for tomographic data sets of already existing experimental stations dedicated to SR CT. In our experimental local CT setup, the specimen was bigger than the FOV perpendicular to the rotation axis and therefore only a portion of the whole sample was assessed. This allowed for high-resolution CT without destruction of the specimen. However, the major problem with local CT measurements is the loss of information required by theory for a proper reconstruction of the specimen's density function, which is a direct consequence of the partial recording of the sample projections. In contrast, the sample projections are captured entirely in the case of a standard (i.e., global) CT setup, and correct reconstruction of the specimen is feasible [14]. In this regard, several mathematical local tomographic methods have been derived to localize the reconstruction [10], which entail only integrals over lines close to the point to be reconstructed. However, these local tomographic methods never reconstruct the original density function of the specimen, but only related functions which behave similarly. Especially for hard tissues, i.e., for highly absorbing X-ray materials, such as bone, residual contrast errors (contrast anomalies) within the reconstructed images can hamper their interpretation [5]. Furthermore, mathematical local tomographic methods

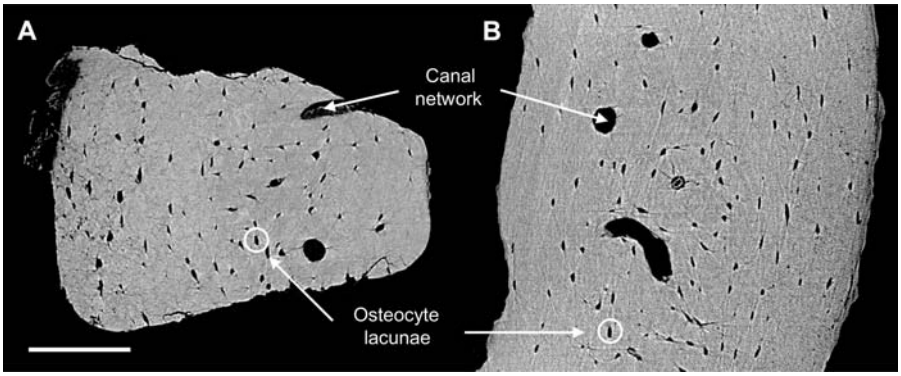

Figure 1 Artifacts arising from mechanical cutting of bone tissue.
(A, B) Reconstructed slices of a cortical sector from two murine femoral mid-diaphyses. Scale bar is 100 μm. (A) Microfractures, fractures, and separate bone fragments owing to mechanical cutting of the bone tissue are clearly visible. (B) The specimen remained intact due to the presented post-processing technique for local synchrotron radiation (SR)-based CT, which allowed for non-destructive assessment, quantification, and subsequent morphometric analysis of bone ultrastructure down to a cellular level. (Methods) The local SR CT measurements were performed in air at the X-ray Tomographic Microscopy (XTM) station [29] of the Materials Science (MS) beamline at the Swiss Light Source (SLS). A total of 1001 projections were acquired over a range of 180 degrees at a photon energy of 17.5 keV and at a theoretical pixel size of 350 nm. The projections were reconstructed using filtered backprojection for parallel-beam geometry. A sinogram-based algorithm was devised to eliminate ring artifacts, which arose from defects on the scintillator of the optical system at the XTM station and which were clearly visible in the reconstructed slices. To partially suppress noise within the reconstructed tomographic data sets, a constrained Gaussian filter was applied.

have not been established as a standard method up to now, such as the conventional filtered backprojection (FBP) for global CT as introduced by Shepp and Logan [25]. For these reasons, they have been used only infrequently for medical imaging [2, 16, 28] and will not be investigated further in this study.

In this study, we introduced a pragmatic method correcting for cupping [9]. Cupping is the most prominent contrast anomaly in local tomographic data sets reconstructed using FBP, as in this study. More precisely, this refers to the effect that for local CT measurements, fractions of the sample outside of the FOV are not reconstructed, but add image energy during FBP, which finally lead to a radial increase of the gray values towards the edge of the reconstruction circle. This effect is shown in Figure 2, where we measured the trabecular compartment of a canine lumbar vertebra with our local SR CT setup at a theoretical pixel size of 350 nm, including subsequent two-fold binning. For 3D analysis and visualization, segmentation of the gray scale image data is necessary. Nevertheless, typical segmentation schemes, such as global thresholding, fail when cupping is present (Figure 2). As a consequence, morphometric quantification of the binarized bone ultrastructure is no longer feasible. There is no theoretical basis for determining analytically the necessary cupping correction [8] when using local tomography reconstruction theory [8–10]. For this reason, we heuristically quantified the cupping effect using cylindrical aluminum phantoms, which were measured in a similar manner. The diameter of phantom 1 (0.5 mm) was chosen to be smaller than the lateral extension of the FOV (0.76 mm), whereas phantom 2 (diameter = 1.5 mm) was designed to exceed the FOV. Accordingly, phantom 1 was measured using a conventional, i.e., global tomographic setup, while phantom 2 was measured locally. Cupping was quantified by calculating the gray value of phantom 2 depending on the distance from the reconstruction center (midpoint) and by averaging the obtained values for 1006 consecutive reconstructed slices. The resulting gray value profile was flat for phantom 1 as expected (Figure 3A). For phantom 2, cupping was described by a radial second degree polynomial gradient (RPG) with $R^2 = 0.99$. For actual cupping correction, the coefficients of the RPG were determined

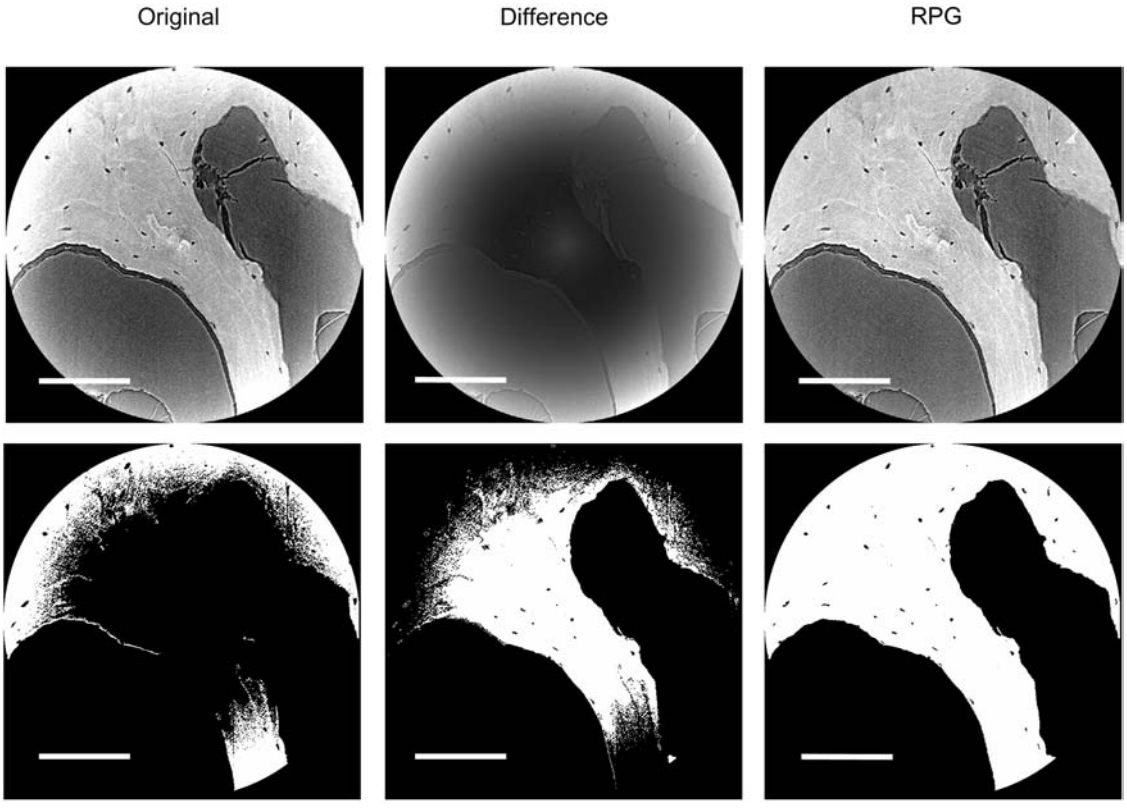

Figure 2 Radial gray value profile correction for local synchrotron radiation-based CT.
(Upper and lower row) All scale bars are 200 μm. (Upper row) Gray-valued reconstructions and (lower row) binarized reconstructions after global thresholding. (Original) Reconstructed slice of the trabecular compartment of a canine lumbar vertebra. The effect of increased gray values for larger radial distances from the reconstruction center (midpoint) is called "cupping" and is due to the local tomographic measurement setup. Segmentation by global thresholding was not successful due to cupping. (RPG) Reconstructed slice after radial polynomial gradient (RPG) correction. The radial gray value profile became flat compared to the original reconstruction. Bone segmentation using global thresholding was now feasible due to the implemented RPG correction. (Difference) The difference between the original and the corrected reconstructions shows the effect of cupping. (Animals and methods) The beagle dog was raised at Indiana University School of Medicine's Assessment of Laboratory Animal Care-accredited facility (Indianapolis, IN, USA) and was sacrificed at the age of 1 year. The cranial portion of the third lumbar vertebra (L3) of the dog was dissected and stored for analysis. All procedures were approved by the Indiana University School of Medicine Animal Care and Use Committee. The measurement protocol is given in the caption of Figure 1, where the data were additionally binned twice to increase the signal-to-noise ratio, resulting in a theoretical pixel size of 700 nm.

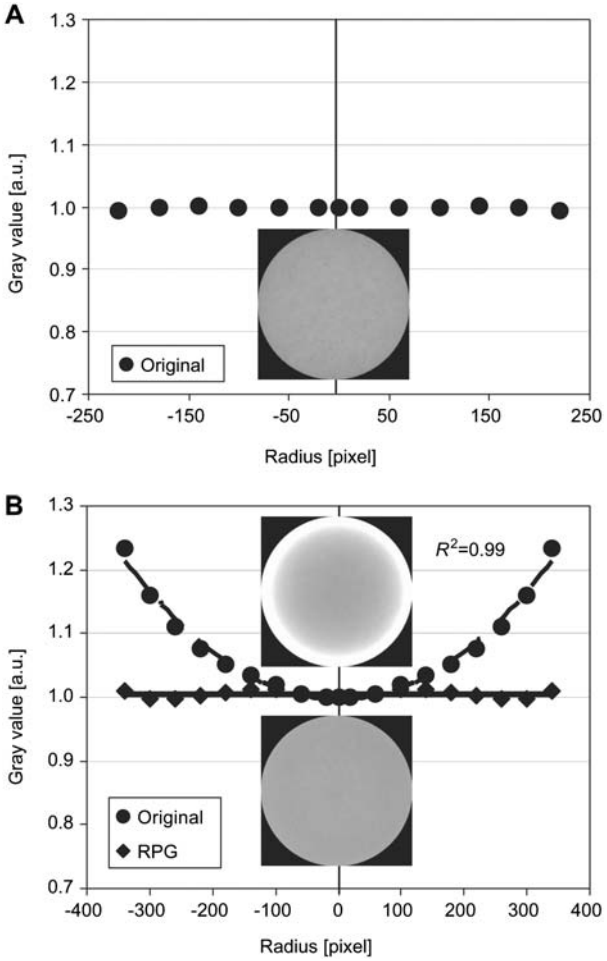

Figure 3 Radial gray value profiles of the phantoms including one reconstructed slice.
(A) Phantom 1, which was measured using a standard, i.e., global tomographic setup since the radial extension (0.5 mm) was smaller than the lateral extension of the acquired projections (0.76 mm). (B) Phantom 2, which was measured using a local tomographic setup because the radial extension (1.5 mm) was bigger than the lateral extension of the acquired projections (0.76 mm). The radial gray value profile together with one reconstructed slice is shown for the original reconstructed data set before ("Original") and after ("RPG") radial polynomial gradient (RPG) correction. The parabolic cupping of the uncorrected data set is visible, which is due to the local tomographic experimental setup.

by an implementation of the Levenberg-Marquardt nonlinear least squares algorithm [18]. Subsequently, the calculated polynomial was used to remove the RPG within the original reconstructions from local CT measurements. Figure 3B illustrates the parabolic and the flat gray value profile of phantom 2 before and after RPG correction, respectively. In addition, the histograms of phantom 2 before and after RPG correction are given in Figure 4. Based on these histograms, Pearson's first coefficient of skewness [$skew_{Pearson,1}$ = (mean-mode)/standard deviation] as a measure of asymmetry and the kurtosis (*kurt*) as a measure of peakedness were calculated. The lopsided histogram ($skew_{Pearson,1}$ = 0.52) of the uncorrected phantom 2 (Figure 4, "Original") caused by the radial gradient was successfully balanced ($skew_{Pearson,1}$ = -0.06) after RPG correction (Figure 4, "RPG"). Furthermore, the

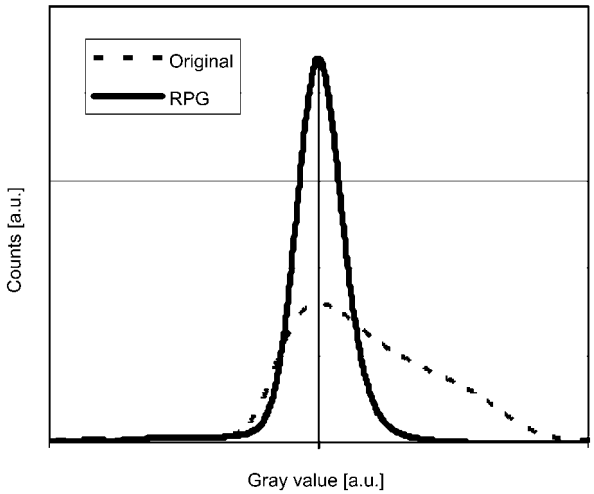

Figure 4 Histograms of the reconstructed phantom 2.
Compared to the original reconstruction ("Original") the distribution of the gray values after RPG correction ("RPG") was balanced and narrowed, which demonstrates that the radial gradient caused by the local tomographic experimental setup was removed successfully, as previously indicated in Figure 3B.

kurtosis of the originally reconstructed phantom 2 (*kurt* = 6.98) was increased by a multiple after correction (*kurt* = 40.77), reflecting the homogenization of the gray value distribution shown in Figure 3B. A similar cupping behavior (R^2 = 0.99) was found for the trabecular compartment of a canine lumbar vertebra (Figure 2), where 256 consecutive reconstructed slices were averaged. To verify this result, we scanned the mid-diaphyseal cortical bone of seven C3.B6-*Ghrhr*^{lit}/J (C3.B6-*lit*/*lit*) mouse specimens at four different anatomical sites (anterior, posterior, lateral, and medial) with the same setup and we evaluated the gray value profile of all 28 measurements in a similar manner. For all these data sets, the radial gray

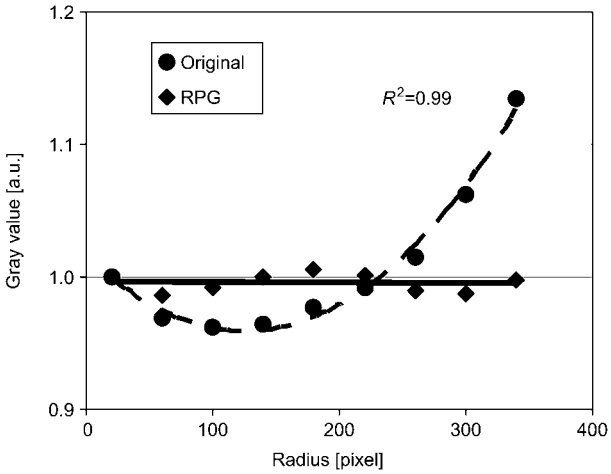

Figure 5 Radial gray value profile within reconstructed bone tissue assessed by local synchrotron radiation-based CT. Radial gray value profile for the original reconstructed data set of the trabecular compartment of a canine lumbar vertebra is shown in Figure 2 ("Original"), and for the same data set after radial polynomial gradient (RPG) correction depicted in Figure 2 ("RPG"). The radial gray value profile of the original tomographic data set ("Original") described by a second degree polynomial became flat after RPG correction ("RPG").

value profile could be characterized by a second degree polynomial ($0.98 \leq R^2 \leq 0.99$) similar to that previously found for the phantom and the canine vertebral bone. In a next step, we performed the RPG correction for the reconstructed canine trabecular bone compartment. In comparison with the original reconstruction (Figure 2, "Original"), the radial gray value profile became flat, which is illustrated in Figure 5. Finally, global thresholding yielded accurate segmentation (Figure 2, "RPG") and allowed for potential quantitative morphometric analysis of the bone ultrastructure. To summarize these results, a post-processing technique for local SR CT was devised, which provides for the first time a method for the non-destructive assessment and quantitative evaluation of hard tissues in the submicrometer domain for reasonably sized specimens.

As a first application of the novel technique for local SR CT, we addressed our original problem, where the ultrastructural examination of murine bone failed because of deterioration of the bone tissue owing to mechanical cutting, which was a requirement for conventional, i.e., global CT in the submicrometer regime. We measured locally the femoral mid-diaphysis of one C3.B6-*lit/lit* mouse and disentangled the intracortical porosity into the canal network and the osteocyte lacunar system as previously described [24]. Figure 6A–C reveals the close entanglement of the canal network (tubes in red) and the osteocyte lacunae (prolate ellipsoids in yellow) within cortical bone (semitransparent envelope). Prepared in this manner, the canal network and the osteocyte lacunar system are ready for quantitative morphometry and with that they constitute ultrastructural phenotypes, which are

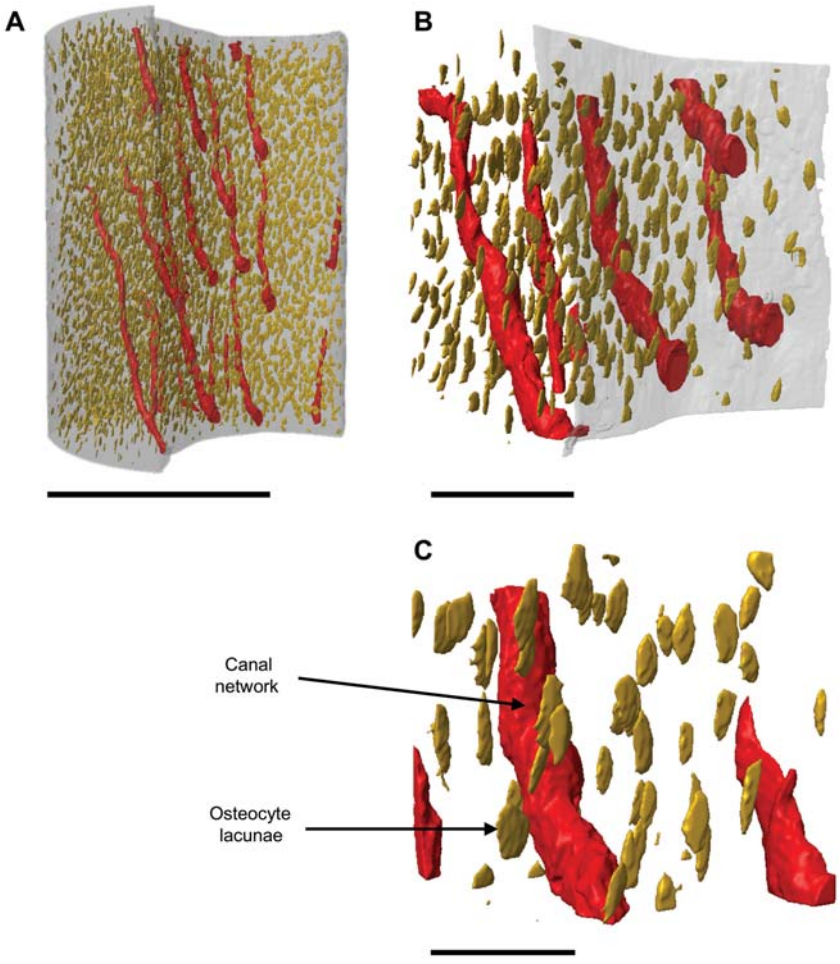

Figure 6 Ultrastructural phenotypes within murine cortical bone.
(A–C) The image shows the canal network (tubes in red) and osteocyte lacunae (prolate ellipsoids in yellow) within the femoral mid-diaphysis of a C3.B6-*Ghrhr*^{lit}/J (C3.B6-*lit/lit*) mouse at different length scales. Scale bars are 500 μm, 50 μm, and 25 μm for panels A, B, and C, respectively. (Animals and methods) Seven C3.B6-*lit/lit* mice were provided by The Jackson Laboratory (Bar Harbor, ME, USA), respectively. Upon necropsy at 16 weeks one femur of each specimen was dissected and stored for analysis. All animal procedures were approved by the Jackson Laboratory's Animal Care and Use Committee. The measurement protocol is given in the caption of Figure 1, where the data were additionally binned twice to increase the signal-to-noise ratio, resulting in a theoretical pixel size of 700 nm. Additionally, iterative global thresholding [17] provided binarized data sets separating bone matrix from soft tissue and air. Negative imaging was previously described [24] and was applied here to assess the porosity within murine cortical bone. In this context, negative imaging denotes the technique to first measure the matrix of a porous structure using CT, and subsequently to extract the enclosed porosity as a negative imprint of the surrounding matrix. In this study, the extraction of the cortical void spaces comprised a combination of different image processing procedures using IPL software (Scanco Medical AG, Brüttisellen, Switzerland), including morphological operators. They were optimized to extract the canal network and the osteocyte lacunar system within cortical bone as two separate phases.

inaccessible to date in 3D and without image artifacts using traditional imaging methods, such as histology and confocal laser scanning microscopy. Consequently, the delineated strategy for local submicrometer SR CT pushes the frontiers of 3D quantitative morphometry to the cellular level in biological samples of relevant object size. In addition, our approach is applicable to new developments towards nano-computed tomography [3, 30] and therefore provides the prerequisite for non-destructive and quantitative 3D investigations of hard tissues with unprecedented resolutions of 100 nm and below.

The technical problem of cupping is quite prominent in the CT literature. Laterally clipped CT data pose a problem in clinical CT or positron emission tomography, where large patients tend to exceed the 50 cm diameter of today's scanners FOV. The state-of-the-art solution to this clipping problem is to extend the projection data laterally and to extrapolate the data smoothly down to zero [11, 19, 22, 27]. All these methods were based on raw data (projections) and they were developed for polychromatic clinical cone beam CT, where the absorption and geometry of the patient's truncated adipose tissue outside of the FOV is estimated. Another raw data-based method [13] to correct for cupping induced by scattering and beam hardening strives to linearize the X-ray attenuation using a pre-correction function, which is determined using a calibration scan of a homogeneous phantom. In contrast to these methods, our correction has been developed for data sets of monochromatic SR-based parallel CT applied to hard tissues, such as bone in the submicrometer regime, where scattering and beam hardening is not an issue and where no prior phantom data are required. Furthermore, our correction for cupping caused by a local tomographic setup is applied on reconstructed and not on raw data, which is why it is a straightforward method to implement. The only comparable post-reconstruction method found in the literature was specifically designed for cone beam breast CT [1], where the focus was to design a correction for the background uniformities due to scattering.

As a limitation of our approach, it should be noted that the presented correction method for cupping artifacts induced by a local tomographic setup is by a design well suited for objects with a rather uniform X-ray attenuation distribution, such as cortical bone. Consequently, SR CT measurements of highly heterogeneous phantoms should be performed in the future to quantify to what extent the application of the proposed method can be expanded to objects with a more complicated X-ray attenuation distribution.

In conclusion, a correction algorithm for local SR CT has been devised which tackles for the first time the existing object size limitation encountered in conventional CT setups for submicrometer imaging of hard tissues. Our technique offers a strategy for SR CT assessment and quantitative analysis of intact specimens larger in size than the reconstruction circle in a truly 3D fashion and at unprecedented resolutions in the submicrometer regime.

Acknowledgements

We are indebted to Dr. Leah Rae Donahue for contributing the mice and we thank Dr. Matthew R. Allen and Dr. David B. Burr for providing the canine bone specimen. Furthermore, we would like to thank Peter Schwilch for the manufacturing of the phantoms. This study was supported by the Swiss National Science Foundation (SNF) through the SNF Professorship in Bioengineering (FP 620-58097.99 and PP-104317/1).

References

[1] Altunbas MC, Shaw CC, Chen L, et al. A post-reconstruction method to correct cupping artifacts in cone beam breast computed tomography. Med Phys 2007; 34: 3109–3118.

[2] Anastasio MA, Shi DX, Pan XC, Pelizzari C, Munro P. A preliminary investigation of local tomography for megavoltage CT imaging. Med Phys 2003; 30: 2969–2980.

[3] Baruchel J, Buffiere JY, Cloetens P, et al. Advances in synchrotron radiation microtomography. Scr Mater 2006; 55: 41–46.

[4] Bousson V, Peyrin F, Bergot C, Hausard M, Sautet A, Laredo JD. Cortical bone in the human femoral neck: three-dimensional appearance and porosity using synchrotron radiation. J Bone Miner Res 2004; 19: 794–801.

[5] Chun IK, Cho MH, Lee SC, Cho MH, Lee SY. X-ray microtomography system for small-animal imaging with zoom-in imaging capability. Phys Med Biol 2004; 49: 3889–3902.

[6] Cooper DM, Turinsky AL, Sensen CW, Hallgrimsson B. Quantitative 3D analysis of the canal network in cortical bone by micro-computed tomography. Anat Rec B New Anat 2003; 274: 169–179.

[7] Donoghue PCJ, Bengtson S, Dong XP, et al. Synchrotron X-ray tomographic microscopy of fossil embryos. Nature 2006; 442: 680–683.

[8] Faridani A, Ritman EL, Smith KT. Examples of local tomography. SIAM J Appl Math 1992; 52: 1193–1198.

[9] Faridani A, Finch DV, Ritman EL, Smith KT. Local tomography II. SIAM J Appl Math 1997; 57: 1095–1127.

[10] Faridani A, Buglione KA, Huabsomboon P, Iancu OD, McGrath J. Introduction to local tomography. In: Quinto ET, Ehrenpreis L, Faridani A, Gonzalez F, Grinberg E, editors. Radon transforms and tomography. Contemporary mathematics, vol. 278. Providence, RI: American Mathematical Society 2001: 29–47.

[11] Hsieh J, Chao E, Thibault J, et al. A novel reconstruction algorithm to extend the CT scan field-of-view. Med Phys 2004; 31: 2385–2391.

[12] Jones AC, Sheppard AP, Sok RM, et al. Three-dimensional analysis of cortical bone structure using X-ray micro-computed tomography. Physica A 2004; 339: 125–130.

[13] Kachelriess M, Sourbelle K, Kalender WA. Empirical cupping correction: a first-order raw data precorrection for cone-beam computed tomography. Med Phys 2006; 33: 1269–1274.

[14] Kak AC, Slaney M. Principles of Computerized Tomographic Imaging. New York: IEEE Press 1988.

[15] Koch A, Raven C, Spanne P, Snigirev A. X-ray imaging with submicrometer resolution employing transparent luminescent screens. J Opt Soc Am A Opt Image Sci Vis 1998; 15: 1940–1951.

[16] Laib A, Rüegsegger P. Local X-ray tomography for in vivo bone structure examinations. Med Phys 1999; 26: 447–452.

[17] Leung CK, Lam FK. Performance analysis for a class of iterative image thresholding algorithms. Pattern Recognit 1996; 29: 1523–1530.

[18] Lourakis MIA. levmar: Levenberg-Marquardt nonlinear least squares algorithms in C/C++. http://www.ics.forth.gr/~lourakis/levmar/; version 2.1.3.

[19] Maltz JS, Bose S, Shukla HP, Bani-Hashemi AR. CT truncation artifact removal using water-equivalent thicknesses derived from truncated projection data. Conf Proc IEEE Eng Med Biol Soc 2007; 2007: 2907–2911.

[20] Martin T, Koch A. Recent developments in X-ray imaging with micrometer spatial resolution. J Synchrotron Radiat 2006; 13: 180–194.
[21] Müller R, Van Campenhout H, Van Damme B, et al. Morphometric analysis of human bone biopsies: a quantitative structural comparison of histological sections and micro-computed tomography. Bone 1998; 23: 59–66.
[22] Ohnesorge B, Flohr T, Schwarz K, Heiken JP, Bae KT. Efficient correction for CT image artifacts caused by objects extending outside the scan field of view. Med Phys 2000; 27: 39–46.
[23] Prymak O, Tiemann H, Sotje I, et al. Application of synchrotron-radiation-based computer microtomography (SRmicroCT) to selected biominerals: embryonic snails, statoliths of medusae, and human teeth. J Biol Inorg Chem 2005; 10: 688–695.
[24] Schneider P, Stauber M, Voide R, Stampanoni M, Donahue LR, Müller R. Ultrastructural properties in cortical bone vary greatly in two inbred strains of mice as assessed by synchrotron light based micro- and nano-CT. J Bone Miner Res 2007; 22: 1557–1570.
[25] Shepp LA, Logan BF. The Fourier reconstruction of a head section. IEEE Trans Nucl Sci 1974; 21: 21–43.
[26] Snigireva I, Snigirev A. X-ray microanalytical techniques based on synchrotron radiation. J Environ Monit 2006; 8: 33–42.
[27] Sourbelle K, Kachelriess M, Kalender WA. Reconstruction from truncated projections in CT using adaptive detruncation. Eur Radiol 2005; 15: 1008–1014.
[28] Spyra WJT, Faridani A, Smith KT, Ritman EL. Computed tomographic imaging of the coronary arterial tree – use of local tomography. IEEE Trans Med Imaging 1990; 9: 1–4.
[29] Stampanoni M, Borchert G, Wyss P, et al. High resolution X-ray detector for synchrotron-based microtomography. Nucl Instrum Methods Phys Res A 2002; 491: 291–301.
[30] Stampanoni M, Borchert G, Abela R, Rüegsegger P. Nanotomography based on double asymmetrical Bragg diffraction. Appl Phys Lett 2003; 82: 2922–2924.
[31] Thurner P, Müller R, Raeber G, Sennhauser U, Hubbell J. 3D morphology of cell cultures: a quantitative approach using micrometer synchrotron light tomography. Microsc Res Tech 2005; 66: 289–298.

Received February 4, 2008; accepted October 10, 2008